



This is a repository copy of *An investigation of the relationship between wear and contact force for abradable materials*.

White Rose Research Online URL for this paper:
<http://eprints.whiterose.ac.uk/92789/>

Version: Accepted Version

Article:

Fois, N., Watson, M., Stringer, J. et al. (1 more author) (2015) An investigation of the relationship between wear and contact force for abradable materials. Proceedings of the Institution of Mechanical Engineers, Part J: Journal of Engineering Tribology , 229 (2). pp. 136-150. ISSN 1350-6501

<https://doi.org/10.1177/1350650114545139>

Reuse

Unless indicated otherwise, fulltext items are protected by copyright with all rights reserved. The copyright exception in section 29 of the Copyright, Designs and Patents Act 1988 allows the making of a single copy solely for the purpose of non-commercial research or private study within the limits of fair dealing. The publisher or other rights-holder may allow further reproduction and re-use of this version - refer to the White Rose Research Online record for this item. Where records identify the publisher as the copyright holder, users can verify any specific terms of use on the publisher's website.

Takedown

If you consider content in White Rose Research Online to be in breach of UK law, please notify us by emailing eprints@whiterose.ac.uk including the URL of the record and the reason for the withdrawal request.



eprints@whiterose.ac.uk
<https://eprints.whiterose.ac.uk/>

An Investigation of the Relationship between Wear and Contact Force for Abradable Materials

N. Fois, J. Stringer, M.B. Marshall

Department of Mechanical Engineering, The University of Sheffield, Mappin Street, Sheffield, S1 3JD, UK.

Abstract

Abradable linings are frequently used on the inside of aero-engine casings. During the operation of engine, the rotating blades may strike the lining of the casing. The wear mechanisms present during these incursions have been re-produced on a scaled test rig platform. Previously, characterisation of the wear has been performed using a stroboscopic imaging technique in order to identify the different wear mechanisms at the incursion conditions investigated. In the present study a dynamometer has been included in the test arrangement allowing the measurement of the contact force. This approach has then been combined with sectioning of the abradable test samples, in order to investigate the material response to the different incursion conditions. The wear results, the cutting force and material structure post-incursion show a high degree of correlation. At low incursion rates, significant consolidation and solidification of abradable material was observed, whilst at the same time adhesive transfer to the blade was recorded along with a low tangential to normal force ratio. At high incursion rates, little solidification and consolidation was observed, together with negligible adhesion and a higher tangential force, suggesting a cutting mechanism. Transitions in material behaviour, wear mechanism, and force ratio were observed at the same incursion condition, further highlighting the link between the different experimental measurements.

Keyword: Abradable, Adhesion, Wear, Aerospace, Force,

1. Introduction

Abradable materials [1-6] are composites used as a lining for casings in aero-engines; they have the ability to be worn by contact with rotating blades but at the same time are erosion resistant. During aero-engine operation, the rotating blades may strike the wall of the surrounding casing. When abradable materials are used as linings, wear is limited to a local area of the coating, and consequently only a local increase in clearance between the blade tip and the lining occurs. Conversely without the use of abradable materials, such a contact causes blade wear, increasing the overall clearance between the blade tips and casing wall, leading to a reduction in the performance of the jet engine.

Previous investigations on abradable materials have included experimental studies that try to replicate in-service conditions, numerical modelling of the contact, and materials testing. In many cases, the experimental studies have focused on creating wear maps, with measurements recorded at the start and end of a given test [7], and as a consequence have failed to accurately investigate the wear mechanisms during an incursion [2]. Typically this has been due to the complexity of instrumenting full-scale test platforms. Similarly, approaches based on numerical modelling [8, 9] have also been limited, due to the lack of detailed experimental data to validate them. Indeed, some of the most complete investigations have focused on materials analysis [10], and whilst being useful in determining mechanical properties, give limited insight into the wear mechanisms observed in service.

Padova et al. [11, 12] analysed the contact force present for a range of incursion conditions using a full-scale test rig, both with the blade striking the casing wall, and with an abradable lining present. During these studies the contact force and temperature, along with the blade displacement were investigated. Whilst the study did not consider wear mechanisms, and focused on large incursion rates, relationships between cutting force and incursion rate were determined. The research highlighted a linear relationship between the load and the incursion rate for low interference between blade and coating, a non-linear transition region as incursion rate increased, followed by an asymptotic region where load showed minimal increase with incursion rate. The influence of blade tip speed was also considered. The amount of material removed radially was reported to decrease with a decrease of the blade speed, with a corresponding increase in the region where a linear relationship between incursion rate and load was present. Overall though, the data set was relatively small, and measured forces were not linked to wear, meaning little insight into the behaviour of abradable materials was attained. Baiz et al. [13] also analysed the dynamic contact between

a flexible blade and abradable coating. During that study, a number of different parameters (incursion speed, number of blade contacts, seal geometry and material removal, normal contact force and blade displacement) were monitored using high-speed videography and force transducers in order to monitor the interaction between the blade and abradable seal. This study highlighted the influence of the incursion depth and incursion speed on the amplitude of blade deflection. The study also showed that surface roughness influenced the degree of the blade deflection. Whilst providing a useful insight, the results were limited by the relatively low blade tip speed (19 m/s) at which tests were performed, and the convex as opposed to aero-engine representative concave contact geometry used.

Metallography, image analysis, X-ray diffraction and electron probe microanalysis [5, 14] are useful techniques that can be used to analyse the composition and structure of abradable materials. Typically this has been done to investigate the performance of different thermal spray conditions, although the techniques are equally applicable to wear investigations. Sample preparation consists of sectioning, mounting and polishing, with the aim of maintaining the original features of the material without introducing cracking or smearing. Vacuum impregnation of pores by epoxy, has been found to increase the contrast of the features within the microstructure when using optical microscopy [15, 16]. However, in order to successfully identify porosity, the contrast and brightness required has been found to be a function of the resolution of the microscope used [17], and in some cases it is still difficult to distinguish between the lubricant phase and porosity even considering this approach.

In this study, a scaled test rig capable of replicating the wear mechanism observed for abradable materials in aero-engines is used to investigate the relationship between contact force and wear over a range of incursion conditions. Previously this test platform has been used to identify the different wear mechanisms present for abradable materials in response to blade strikes, using a stroboscopic imaging technique [1, 2]. Here a piezoelectric dynamometer is added to the test arrangement to measure contact force, with sectioning of the abradable test samples also performed to investigate the material response for the different incursion conditions investigated.

2. Methodology

2.1 Test Rig

The test platform has been described in detail previously, and it has been demonstrated that it is capable of generating similar wear mechanisms to those observed for abradable materials

in an aero-engine [1, 2]. A summary of the test rig is now presented, with specific details given of the changes made for the present study. The test rig is based around a bench-mounted machine tool spindle, which has a maximum rotational speed of 21000 r/min. The spindle is composed of a metal disc, which contains a removable blade specimen along with a dummy blade 180° opposed to it for balancing. An electrical Z-axis microscope stage, mounted below the coating, allows incursions between 0.1-2000 $\mu\text{m/s}$ at intervals of 0.1 $\mu\text{m/s}$ to occur between the blade and coating. The incursion is set at the start of a test using a programmable stage controller. A stroboscopic imaging set-up, described below, is used to image the blade tip during the programmed incursion. Additionally, in this series of experiments, a dynamometer plate is also used to measure the force associated with a blade strike. Through a combination of these two systems, the blade tip can be measured on a pass-by-pass basis, along with the contact force. The temperature of the coating has also been measured during the tests using a laser pyrometer. Figure 1 shows an image of the front of the test rig.

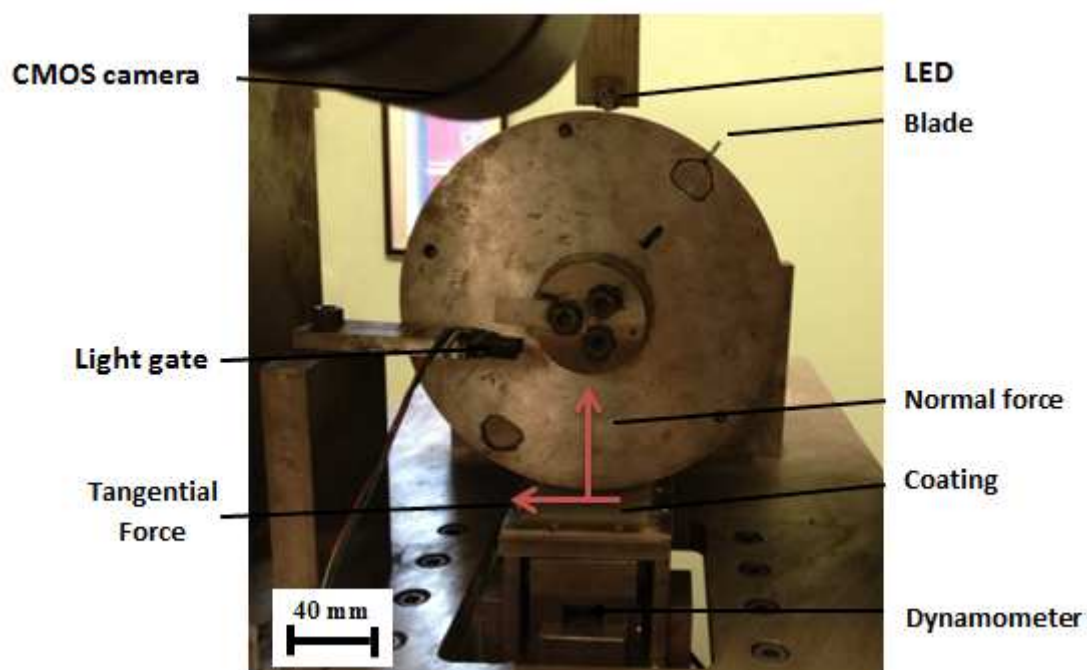


Figure 1. Front Image of the test rig

2.2 Stroboscopic imaging set up

The stroboscopic set up images the blade tip, and allows the investigation of adhesion and wear rates [2]. The set-up is composed of an LED, LED Strobe controller, light gate, and CMOS camera with a macro zoom lens. The system is triggered via interruption of the light

gate, timed so that the LED Strobe generates a pulse of light as the test blade passes the camera, allowing an image to be captured of the blade tip.

2.3 Force measurement

The contact force between the blade and abradable material is measured using a dynamometer (Kistler Instruments Ltd, Hook, (UK), Type 9347 C), connected to a charge amplifier (Kistler Type 5070A), and a digital oscilloscope (Pico Technology 3000 series). This type of dynamometer measures the contact force using a piezoelectric force link. It has a longitudinal contact force range of -5 kN to 5kN, a normal contact force range of -30 kN to 30 kN, with natural frequencies of 3.6 kHz and 10 kHz respectively for the longitudinal and normal axes. The Multichannel charge amplifier (Type 5070A 4 channel) converts the electric charge from the dynamometer to a scaled voltage (Voltage output $\pm 10V$) with a calibration performed prior to testing to determine this relationship. The digital oscilloscope then captures the voltage signal from the charge amplifier, and is able to sample at a rate of 1 GHz with time bases ranging from 2 ns/div to 200 s/div.

2.4 Temperature measurement

As shown in Figure 2, the coating temperature is measured during an incursion using a pyrometer (Micro-epsilon, Koenigbacher, Germany). The pyrometer is an infrared sensor with a spectral range 2.3 μm , capable of measuring temperatures from 150 °C to 1000 °C. The coating temperature has been measured at a single point on the surface of the abradable material where the blade strikes, and average temperatures determined for the different incursion conditions investigated.



Figure 2. Temperature sensor.

2.5 Data Acquisition and Synchronization

The LED was triggered through a rigid metal arm, mounted onto the disk and located so that the light gate was interrupted and generated a trigger pulse, each time the disk revolved. The strobe controller, on receiving the trigger pulse and after an appropriate delay, emitted a high energy – short duration pulse (1 μ s pulse of 48 V and 20 A) to drive the LED. This resulted in a short duration LED flash enabling images of the moving blade to be captured with minimal motion blur.

The normal and the tangential contact force were measured using the dynamometer. The dynamometer was inserted below the abradable coating in order to measure the contact force during each test. As mentioned previously, the digital oscilloscope was used to capture the force output from the dynamometer. The z-axis microscope stage, the camera image acquisition, and the force measurement were controlled via Labview (National Instruments, Labview 2009). In this way, blade tip images and force measurements were captured at known times in the programmed incursion, ensuring synchronisation with respect to the two different data sets. This approach allowed measurements of blade wear or adhesion to be investigated in the context of incursion rate and contact force. Figure 3 shows a schematic diagram of the test rig.

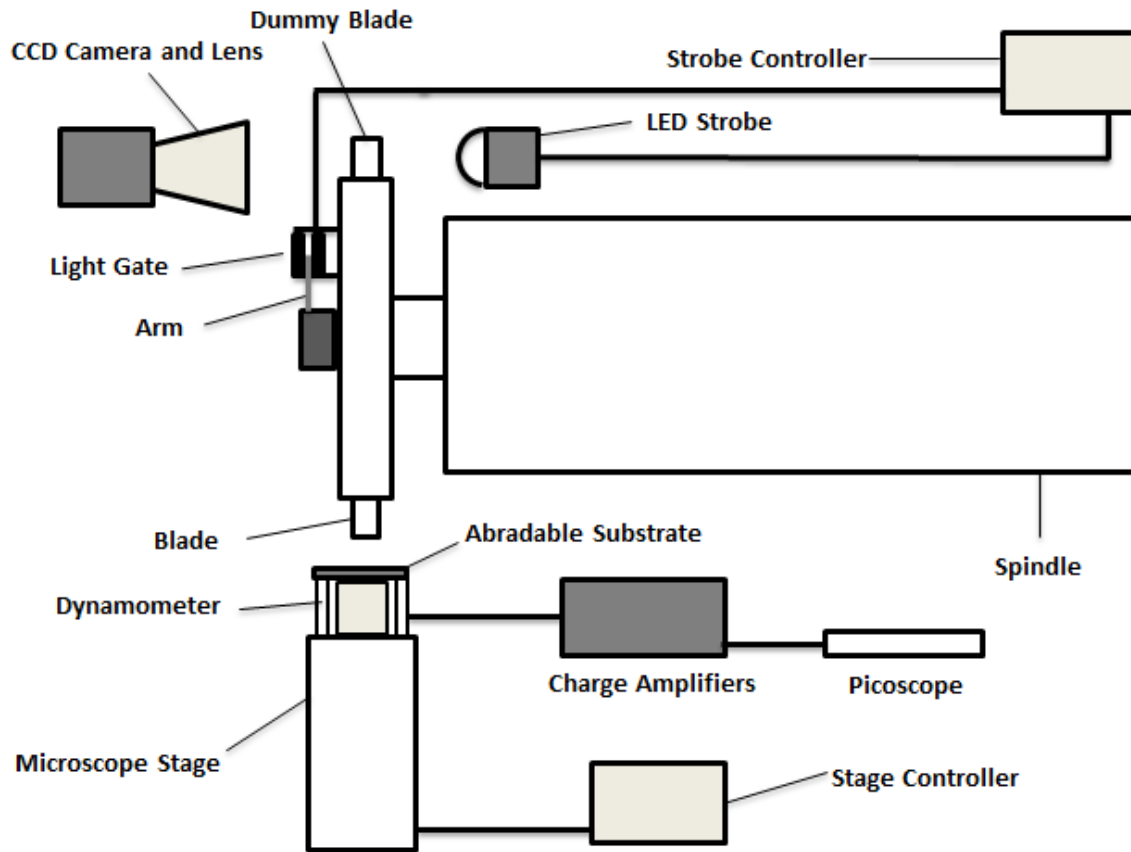


Figure 3. Schematic block diagram of the test rig.

2.6. Test Parameters and Samples

2.6.1. Test Materials

An abrasable material containing aluminium, silicon and hexagonal boron nitride (AlSi-hBN) was thermally sprayed onto a flat steel plate to a nominal thickness of 3 mm. The hardness of the abrasable material supplied was measured using a Rockwell R15Y hardness indenter, and it was found to have an average hardness value of 73 when measured on this scale. In order to test the samples, they were then mounted onto the Z-axis microscope stage. Square edged, flat Titanium blades were manufactured from Ti-6Al-4V, with a nominal length of 25 mm and thickness of 2 mm. Once seated in the spindle tool, the effective blade length outside the rotor was 13 mm. Prior to each test, the length and mass of each blade were recorded.

2.6.2. Test parameters

In the tests performed, the impact velocity was fixed at 100 ms^{-1} and incursion speed varied between $3.4 \text{ } \mu\text{ms}^{-1}$ and $344 \text{ } \mu\text{ms}^{-1}$. The incursion speed is the rate at which the stage motor advances the abrasable sample in the Z-axis direction. Previous research has identified this as

the dominant parameter with respect to the wear mechanics, and that through the range of test conditions selected, similar wear mechanisms to those observed in aero-engines are obtained [1, 2]. Table 1 summarizes the different incursion conditions investigated. As shown in the table, the overall incursion depth was kept constant, and was limited by the thickness of the coating. This in turn also limited the total theoretical length of the rub $L(t)$ (m). This parameter is a combination of the incursion speed I (m/s), time t (s), rotor radius at blade tip R (0.0925 m), and the theoretical number of strikes n , and is calculated as shown in Equation (1).

$$L(t) = \sum_{i=1}^n 2 \cdot R \cdot \arccos\left(\frac{R - I_i \cdot t_i}{R}\right) \quad (1)$$

In order to perform a given test, the required incursion speed was set via the Labview interface. The tests have been performed with a range of incursion speeds between $3.4 \mu\text{ms}^{-1}$ and $344 \mu\text{ms}^{-1}$ to a total incursion depth of 2 mm, with the aim of identifying the incursion conditions at which the wear mechanism transitions from adhesion combined with blade wear to cutting.

Test	Blade Tip velocity [ms^{-1}]	Incursion Speed [μms^{-1}]	Incursion Rate per Pass [μm]	Incursion Depth [μm]	Theoretical Rub Length [m]
1	100	3.4	0.02	2000	2567.5
2	100	6.7	0.04	2000	1283.8
3	100	10.05	0.06	2000	855.84
4	100	16.75	0.1	2000	513.52
5	100	23.45	0.14	2000	366.78
6	100	34	0.2	2000	256.76
7	100	172	1	2000	51.37
8	100	344.1	2	2000	25.69

Table 1. Programmed test parameters.

It should also be noted that the range of incursion speeds was selected based on the incursion per pass, which is defined as the axial depth of material removed by the blade during a single strike of the coating. Figure 4 shows a schematic diagram of the coating section at the end of a test, where the total incursion depth and abraded surface are highlighted.

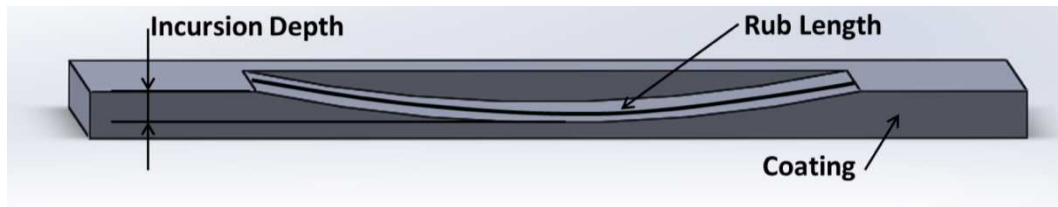


Figure 4. Schematic diagram of the abraded test sample.

2.7. Stroboscopic Imaging Technique Data Analysis

The stroboscopic image analysis allows the blade length to be measured on a pass-by-pass basis. The image analysis steps have been described in detail previously [2]. In order to obtain the blade length change from the acquired images, processing is performed using the software IMAGE-J (a scientific image processing, software package developed by the National Institute of Health based on Sun-Java) in order to determine the blade profile in a cartesian co-ordinate system. The profile of the blade is then analysed using MATLAB (Mathworks, MATLAB R2009a), in order to obtain the maximum length at a given point in the incursion. This value can then be compared to the initial blade length. Using this technique the progressive adhesion or material loss from the blade is characterised as a function of the rub length.

2.8. Force measurement data analysis

The dynamometer produced an electrical signal proportional to the applied force; this value was then amplified by the charge amplifier, before being recorded using the digital oscilloscope. Figure 5a shows a typical force signal recorded for a series of blade strikes on the abradable material. As shown in the figure, a given strike is comprised of a major peak, followed by a period of free vibration prior to the blade re-striking the substrate. Figure 5b shows a single strike on the coating. Highlighted on the figure is the expected contact time based on the blade speed and length of the arc of contact at this point in the incursion. The next stage of the analysis involved investigating the dynamic behaviour of the force measurement system to determine whether compensation was required. As a first step, the contact duration was measured at different points in the incursion and compared against the theoretical value (Figure 5c). As shown in the figure, correlation between the measured and

calculated values was good, and indicates that the blade strike has been correctly identified [18]. Following on from this, modal analysis of the system was performed using an impulse hammer (PCB 086C01, sensitivity 11.65 mV/N, PCB Piezotronic, Inc. USA), accelerometer (PCB 352B10, Sensivity 1.02 mV/m/s², PCB Piezotronic, Inc. USA) and National Instruments data acquisition system (NI USB-4431, 24 bit resolution), and the frequency response function (FRF) of the measurement system was acquired. The inverse transfer function was then used to apply dynamic compensation to the measured force signal [12, 19]. Additionally, accelerometric compensation [20] was also applied to the system, with the specific aim of investigating inertial effects in both the blade contact and free vibration components of the measurement. The compensated and un-compensated measurements are shown in Figure 5d. As shown in the figure, the component of the measurement representing the blade contact did not change (within the accuracy of the FRF and acceleration measurements) with compensation applied, indicating that it is not required in this case.

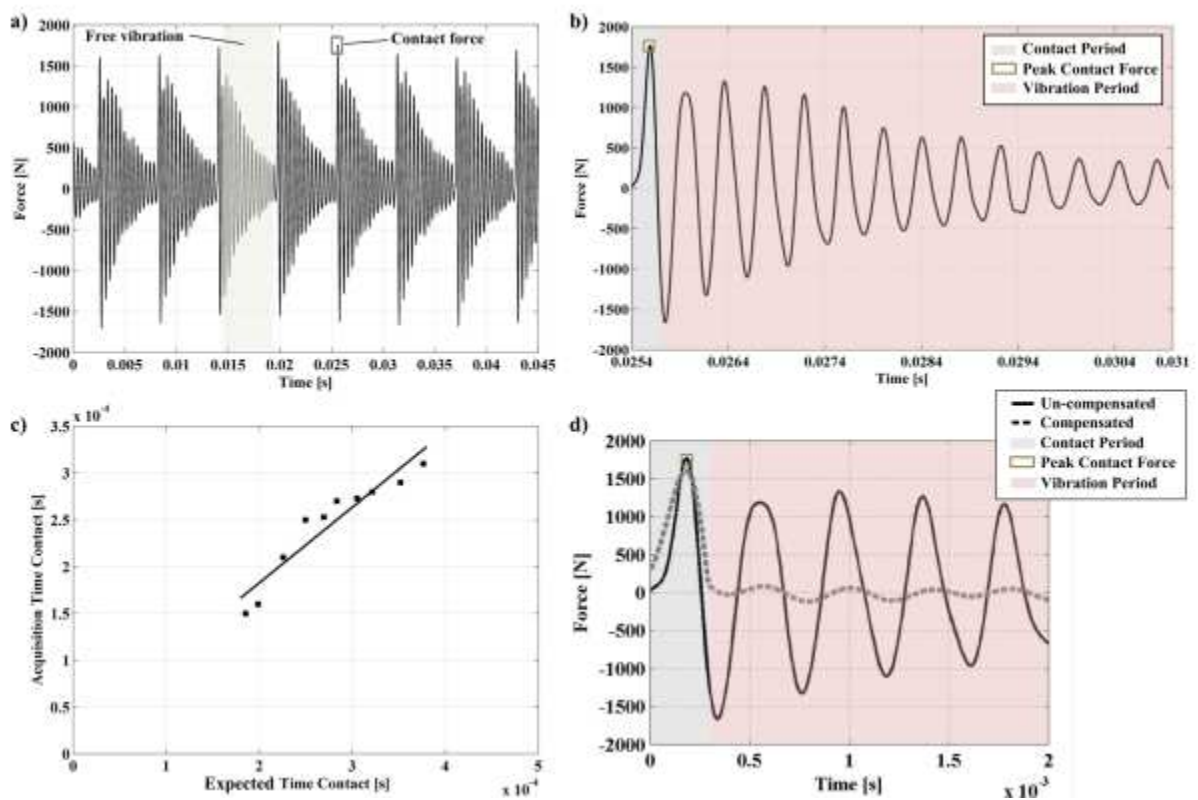


Figure 5. Force measurement (normal component) and analysis: a) recorded for multiple blade strikes; b) single blade strike recorded at time of 0.0254 s; c) expected vs. theoretical contact duration; d) dynamically compensated and un-compensated force measurements.

Measurements recorded for the tangential force were similar in nature, and the blade contact was clearly evident. For a given test, both normal and tangential components of the contact force were measured for each strike, and recorded as a function of rub length.

2.9 Material Sectioning

In order to analyse the structure of the abradable material, the samples were sectioned in both the longitudinal and transverse directions with respect to the blade strike (Figure 6). The samples were mounted and inserted in a vacuum bell for resin impregnation with epoxy resin. This was performed in order to infiltrate any porosity and clearly distinguish between the different features of the coating. Post-impregnation, the samples were placed inside an oven for two hours at 50 °C in order to solidify. Optical Microscopy (Carl Zeiss Axio Scope.A1) was performed at magnifications of x5 and x10.

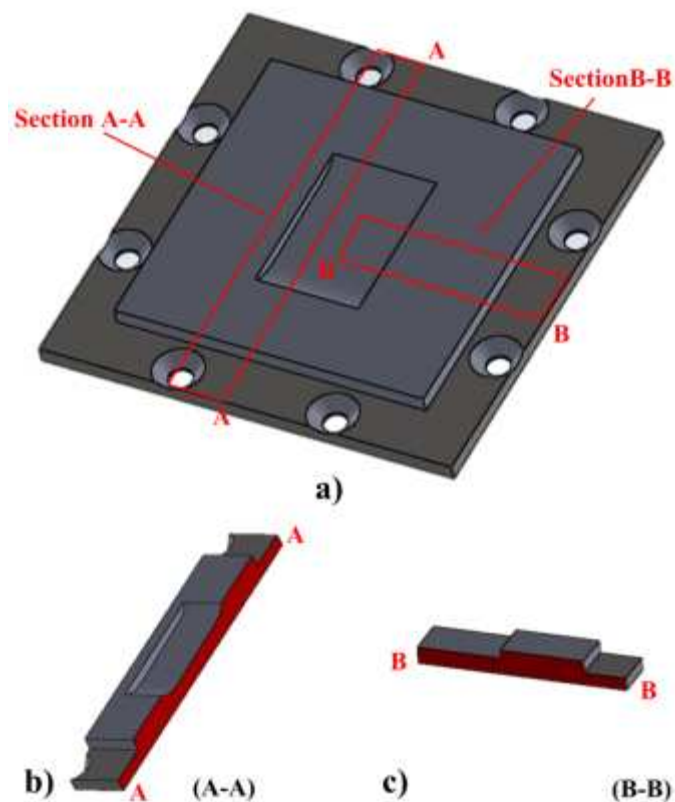


Figure 6. Section of abradable coating: a) coating; b) longitudinal section; c) transverse section.

3. Results

3.1. Wear Mechanism and Adhesion Rate

The main wear mechanisms observed were adhesive transfer from the coating to the blade, or cutting wear. Table 2 summarises the tests performed, highlighting the different wear mechanisms observed. Also included in the table are maximum blade length, normal force and tangential force recorded during a given test.

Test	Blade Tip Speed [ms ⁻¹]	Incursion Rate per pass [μm]	Blade Length change [mm]	Max Normal Force [N]	Max Tangential Force [N]	Average Temp. [°C]	Max Temp. [°C]	Wear Mechanism
1	100	0.02	2.429	1258	151	440.7	509.4	Adhesion / Thermal Damage
2	100	0.04	1.603	1768	650	374.2	457.5	Adhesion
3	100	0.06	0.497	1328	465	350.1	455.7	Adhesion / Cutting wear
4	100	0.1	0.36	1516	543	344.99	415.7	Initial Adhesion / Cutting wear
5	100	0.14	0.29	2564	1335	312.6	436.3	Cutting wear
6	100	0.2	0.227	3222	1316	337.8	438.4	Cutting wear
7	100	1	0.123	4107	2394	338.7	449.3	Cutting wear
8	100	2	0.158	4360	2554	213.9	281.1	Cutting wear

Table 2. Wear mechanism, length change and measured forces with respect to programmed test conditions.

Figure 7a shows a typical result from a test with high levels of adhesion, in this case performed at an incursion rate of 0.02 μm·pass⁻¹ (Test 1). As shown in the image, there is significant adhesive transfer to the blade tip, and also an area of wear accompanied by thermal damage. The adhesive transfer to the blade has resulted in grooving of the coating, with the major peak in the groove pattern corresponding to the location of thermal damage on the blade.

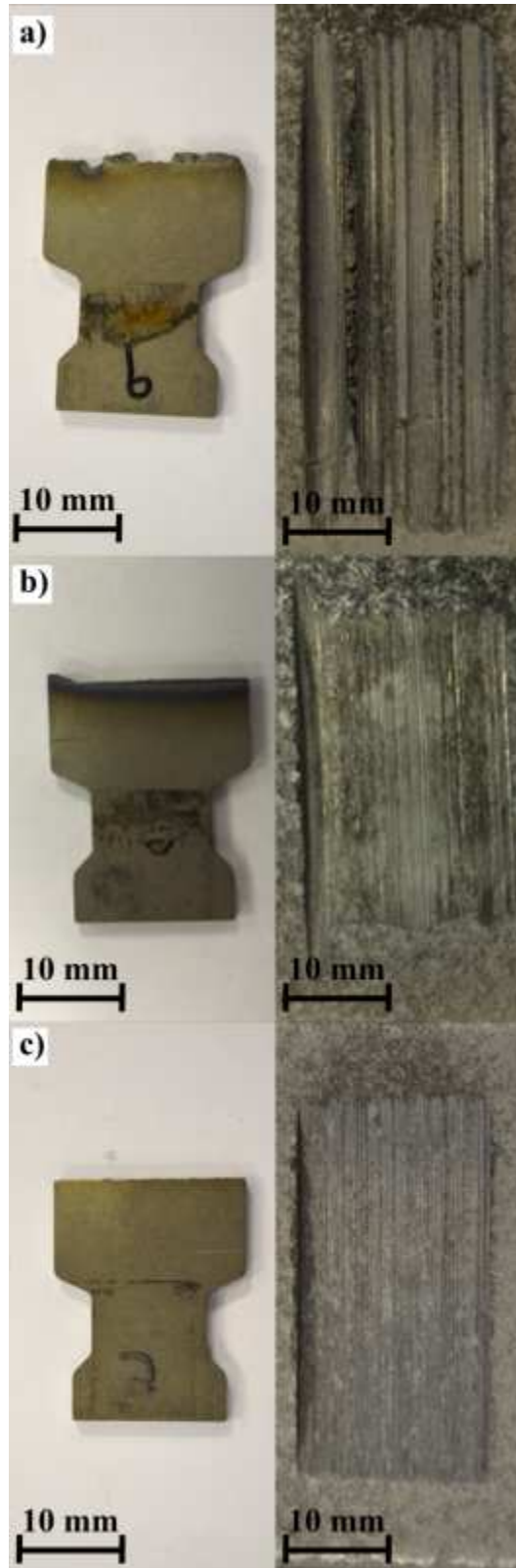


Figure 7. Image of the blade and abradable test specimen post-test for a) an incursion rate of $0.02 \mu\text{m}\cdot\text{pass}^{-1}$ (Test 1); b) an incursion rate of $0.06 \mu\text{m}\cdot\text{pass}^{-1}$ (Test 3); c) an incursion rate of $2 \mu\text{m}\cdot\text{pass}^{-1}$ (Test 8).

Similarly Figure 7c shows the blade and abradable material post-test at an incursion rate of $2 \mu\text{m pass}^{-1}$. At this high incursion rate, the blade was observed to cut the abradable material well, resulting in a lightly grooved surface with a dull appearance. This type of surface is typical of cases where cutting of the abradable material by the blade is reported. As shown, there is also no damage to the blade, with minimal blade wear. At the intermediate incursion rates the wear mechanism was observed to progress from adhesive transfer from the abradable material to the blade, through to clean cutting of the abradable material. Through observing the substrates post-test, this transition was observed to occur at an incursion rate $0.06 \mu\text{m}\cdot\text{pass}^{-1}$ (Test 3), with the corresponding test samples shown in Figure 7b. It is also interesting to note that at low incursion rates where thermal damage and adhesion has been evident, temperatures measured (Table 1) are significantly higher than those when cutting dominates, and that as a general trend temperature is relatively constant once cutting is established.

However, by only observing the specimens at the end of the test, it is not possible to investigate whether a given wear mechanism was present for the full duration of the rub. As mentioned in Section 2.4, the stroboscopic imaging technique can be used to measure the change in blade length dynamically as the incursion test is on-going. Figure 8 shows the change in blade length for the series of different incursion rates tested.

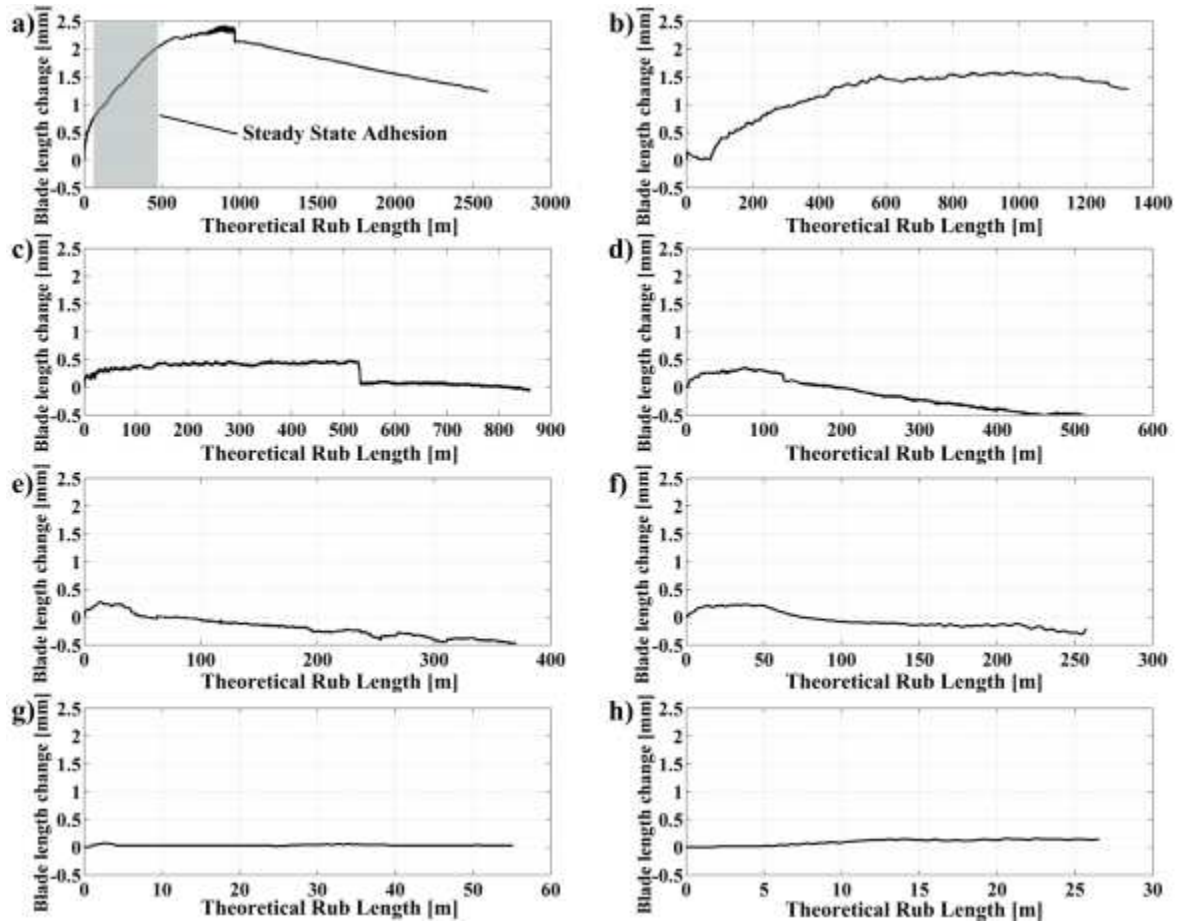


Fig.8. Blade length change expressed in terms of theoretical rub length at incursion rate of: a) $0.02 \mu\text{m}\cdot\text{pass}^{-1}$; b) $0.04 \mu\text{m}\cdot\text{pass}^{-1}$; c) $0.06 \mu\text{m}\cdot\text{pass}^{-1}$; d) $0.1 \mu\text{m}\cdot\text{pass}^{-1}$; e) $0.14 \mu\text{m}\cdot\text{pass}^{-1}$; f) $0.2 \mu\text{m}\cdot\text{pass}^{-1}$; g) $1 \mu\text{m}\cdot\text{pass}^{-1}$; h) $2 \mu\text{m}\cdot\text{pass}^{-1}$.

As shown in the figure, at the lowest incursion rate ($0.02 \mu\text{m}\text{ pass}^{-1}$) significant adhesive transfer from the coating to the blade tip occurs, with the adhered material ultimately partially breaking away. The growth, break away and in some cases re-initiation of adhesion has been previously reported [2], and the result shown here is consistent with this study. Progressively, as the incursion rate increases, the level of adhesive transfer reduces. This is evident when comparing Figures 8a,b and c, which show the transfer at incursion rates of 0.02, 0.04, and 0.06 micrometers per pass (Test 1, 2, and 3 respectively). As shown in Figure 8c, at an incursion rate of 0.06 microns per pass adhesion initially occurs, breaks away and fails to re-initiate resulting in a cut-like appearance on the abrasable surface (Figure 7b). It is also interesting to note in this case that whilst a small amount of blade wear is reported at the end of the test, inspection of the blade tip shows wear mixed with small amounts of residual adhesion, indicating the co-existence of the two mechanisms. Following on from this, as shown in Figure 8d at an incursion rate of 0.1 micrometers per pass (Test 4), initial adhesion

is minimal with a cutting mechanism now dominant. As shown in Figures 8e, f, g, and h, which show the blade length change at incursion rates of 0.14, 0.2, 1 and 2 micrometers per pass respectively (Tests 5, 6, 7 and 8), the cutting mechanism is maintained with minimal blade wear recorded with increasing incursion rate.

Using the measured changes in blade length, an assessment can be made with respect to how the actual rub length compared to the calculated theoretical value. This has been achieved by updating the blade length on a pass-by-pass basis (using the results shown in Figure 8) when calculating rub length using Equation (1). As the camera is side-on and maximum blade lengths are recorded, the calculated rub length is in turn the maximum value experienced along the blade face.

Test	Incursion Rate per Pass [μm]	Calculated Rub Length [m]	Theoretical Rub Length [m]
1	0.02	4328.7	2567.5
2	0.04	1824.5	1283.8
3	0.06	999.0	855.8
4	0.1	519.7	513.5
5	0.14	358.0	366.8
6	0.2	261.6	256.7
7	1	52.4	51.4
8	2	26.6	25.7

Table 3. Theoretical vs. measured rub length with respect to test conditions.

As shown in Table 3, where material adheres to the blade tip rub length is significantly increased, as evidenced by the increased arc of contact on the abradable sample for the low incursion rate test (Figure 8a). However, it should be noted that the maximum length may occur at different points along the blade face during the rub, and in particular in cases where break away of adhered material occurs. Therefore, this actual rub length can only serve as an estimate of the maximum value. Conversely, at all but the most adhesive condition, and in

particular where good cutting is reported, theoretical and actual rub lengths are similar. Thus, theoretical rub length is used in the following analyses.

Adhesive transfer of abradable materials can be characterised by a period of initial growth, followed by a steady-state adhesion. The adhesion rate in the steady state period is calculated as the rate of change of blade length with respect to theoretical rub length [2]. Figure 8a shows an example of the region of steady-state adhesion (grey area), as measured for Test 1 at 0.02 micrometers per pass. A similar analysis was performed for all of the incursion rates investigated, and the adhesion rate was found to rapidly drop as incursion rate increased (Figure 9). Also included in the figure is data recorded in a previous study [2], where a similar relationship was observed to this series of tests. It should be noted in the comparative data that the negative adhesion rate at an incursion rate of 2 micrometres per pass corresponds to blade wear, and that in general the softer coating was characterised by a higher rate of adhesion.

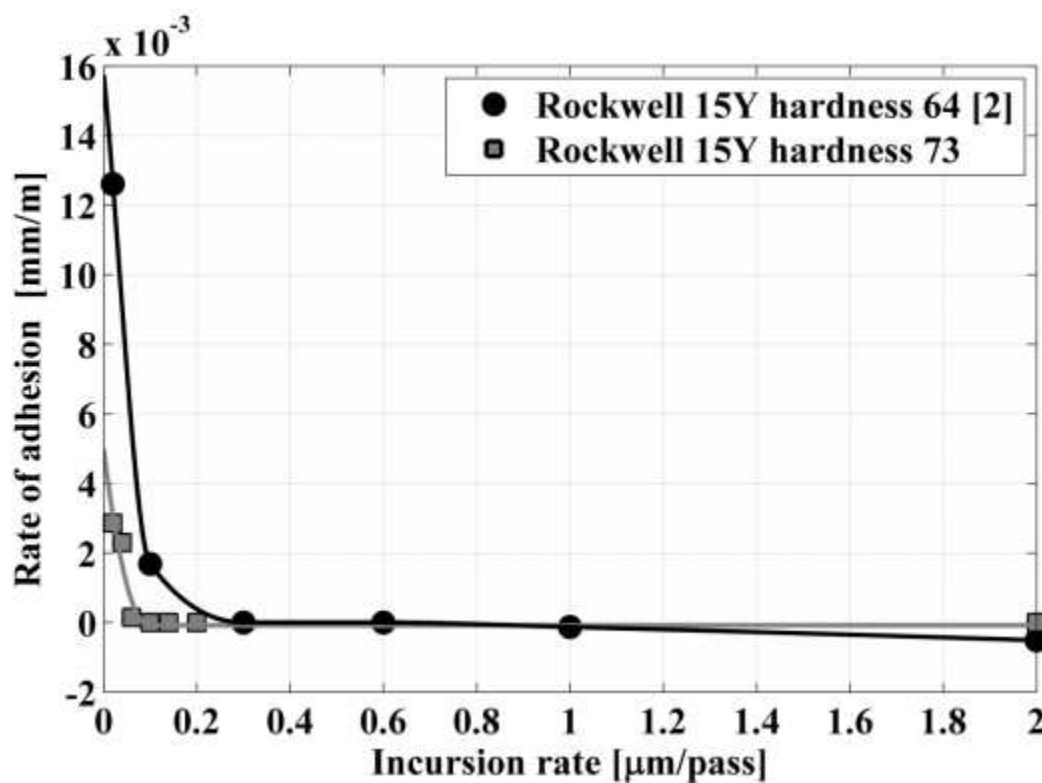


Figure 9. Adhesion rate with respect to incursion rate.

3.2 Force Measurement

Normal and tangential forces were measured during each of the tests performed. Individual blade contacts were captured, with the maximum force during the blade strike plotted as a

function of rub length. Figures 10 and 11 show the normal and tangential forces respectively at low, intermediate and high incursion rates.

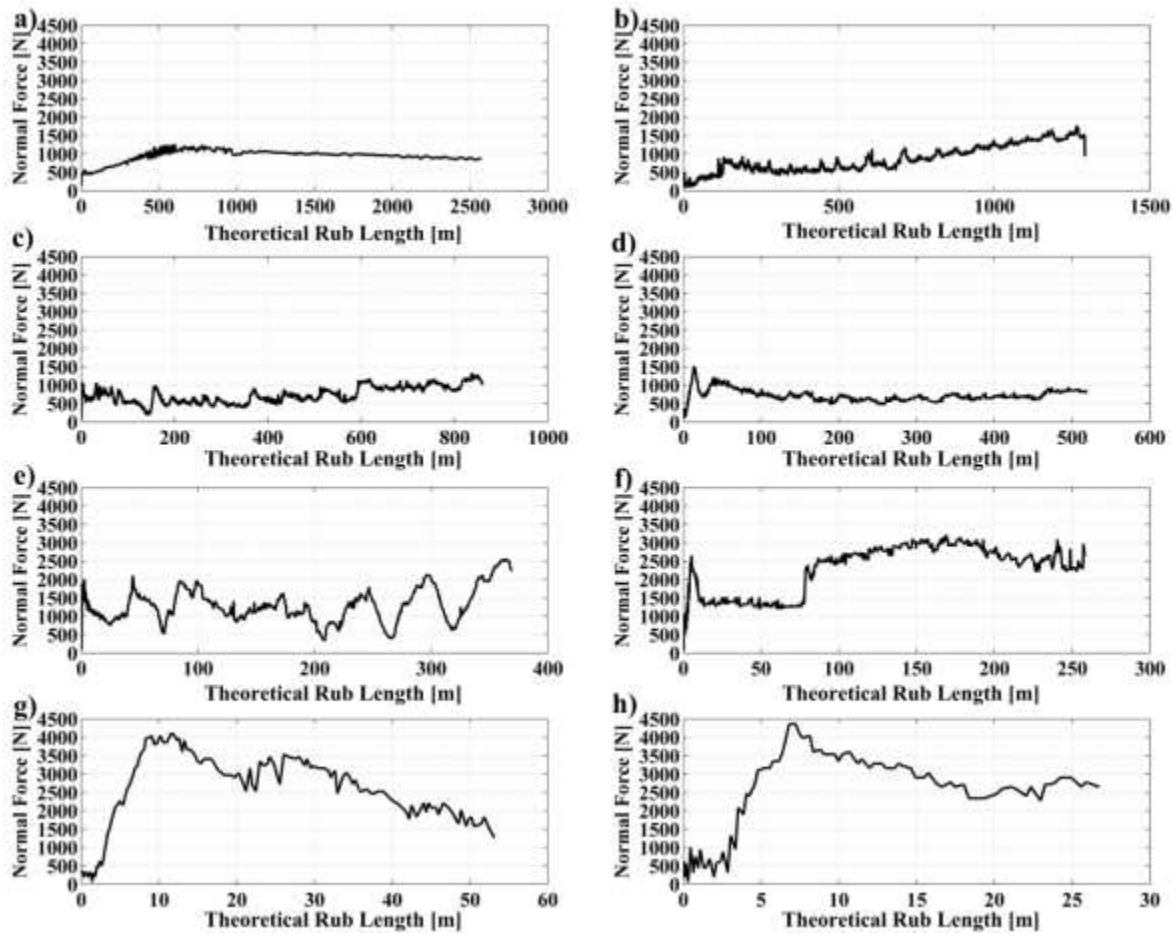


Figure 10. Normal force measurement at incursion rates of: a) $0.02 \mu\text{m}\cdot\text{pass}^{-1}$; b) $0.04 \mu\text{m}\cdot\text{pass}^{-1}$; c) $0.06 \mu\text{m}\cdot\text{pass}^{-1}$; d) $0.1 \mu\text{m}\cdot\text{pass}^{-1}$; e) $0.14 \mu\text{m}\cdot\text{pass}^{-1}$; f) $0.2 \mu\text{m}\cdot\text{pass}^{-1}$; g) $1 \mu\text{m}\cdot\text{pass}^{-1}$; h) $2 \mu\text{m}\cdot\text{pass}^{-1}$.

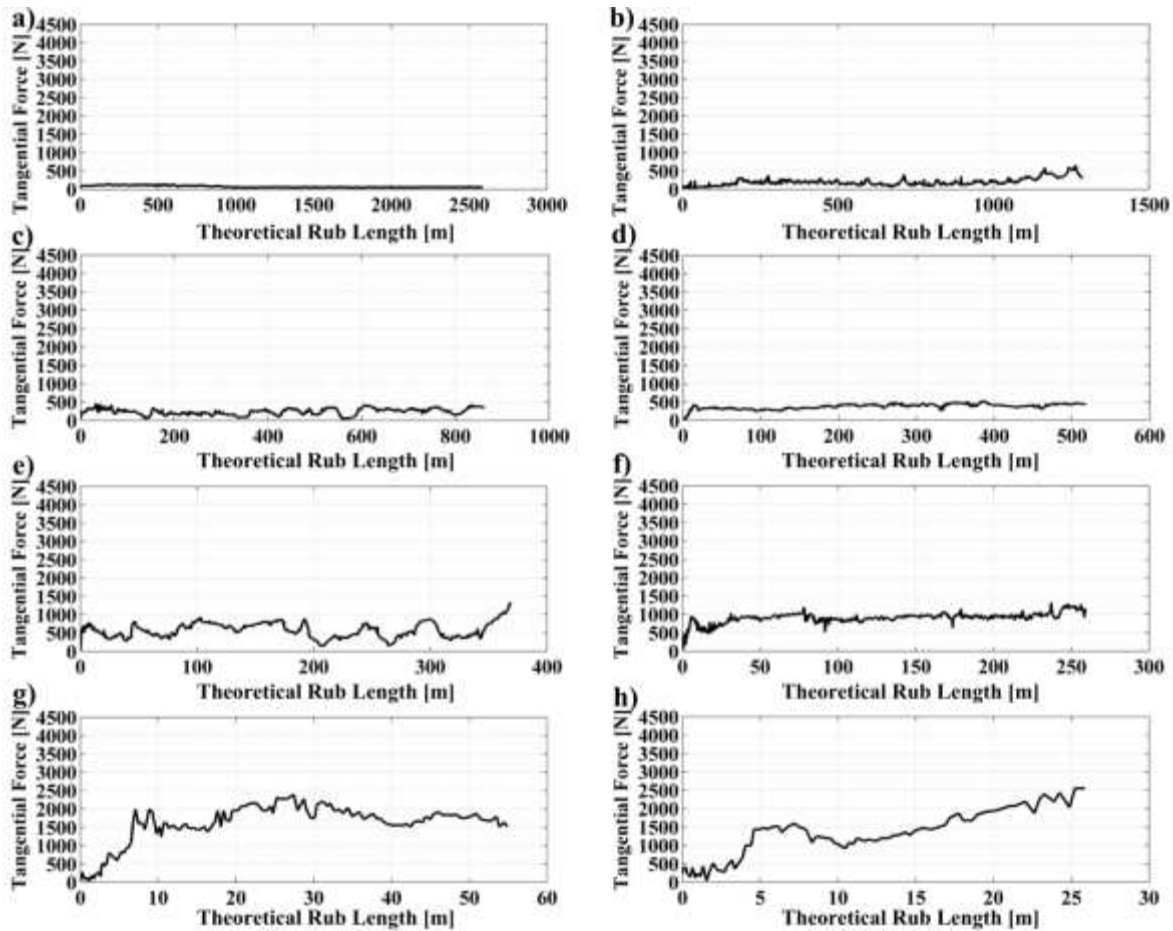


Figure 11. Tangential force measurements at incursion rates of: a) $0.02 \mu\text{m}\cdot\text{pass}^{-1}$; b) $0.04 \mu\text{m}\cdot\text{pass}^{-1}$; c) $0.06 \mu\text{m}\cdot\text{pass}^{-1}$; d) $0.1 \mu\text{m}\cdot\text{pass}^{-1}$; e) $0.14 \mu\text{m}\cdot\text{pass}^{-1}$; f) $0.2 \mu\text{m}\cdot\text{pass}^{-1}$; g) $1 \mu\text{m}\cdot\text{pass}^{-1}$; h) $2 \mu\text{m}\cdot\text{pass}^{-1}$

As shown by both Figures 10 and 11, the normal and tangential forces were subject to significant variation throughout a given test, over the range of incursion conditions investigated. In some cases cutting forces were observed to rise to a maximum, before remaining at a more steady state value for the remainder of the test (eg. Test 1, Figures 10a and 11a respectively). The observed variation in cutting force is expected, particularly when considered in the context of the blade length measurements. As shown in Figure 8, over the range of incursion rates tested, the observed length change showed continuous variation over the rub length. It is also interesting to note that in the case of Test 1 carried out at an incursion rate of $0.02 \mu\text{m}\cdot\text{pass}^{-1}$, the normal force recorded (Figure 10a) shows a similar trend to the result for blade length change shown in Figure 8a. A similar comparison can also be made with respect to the tangential force (Figure 11a), however in this case whilst observable, the trend is less pronounced. In general, both tangential and normal forces were also observed to increase with incursion rate.

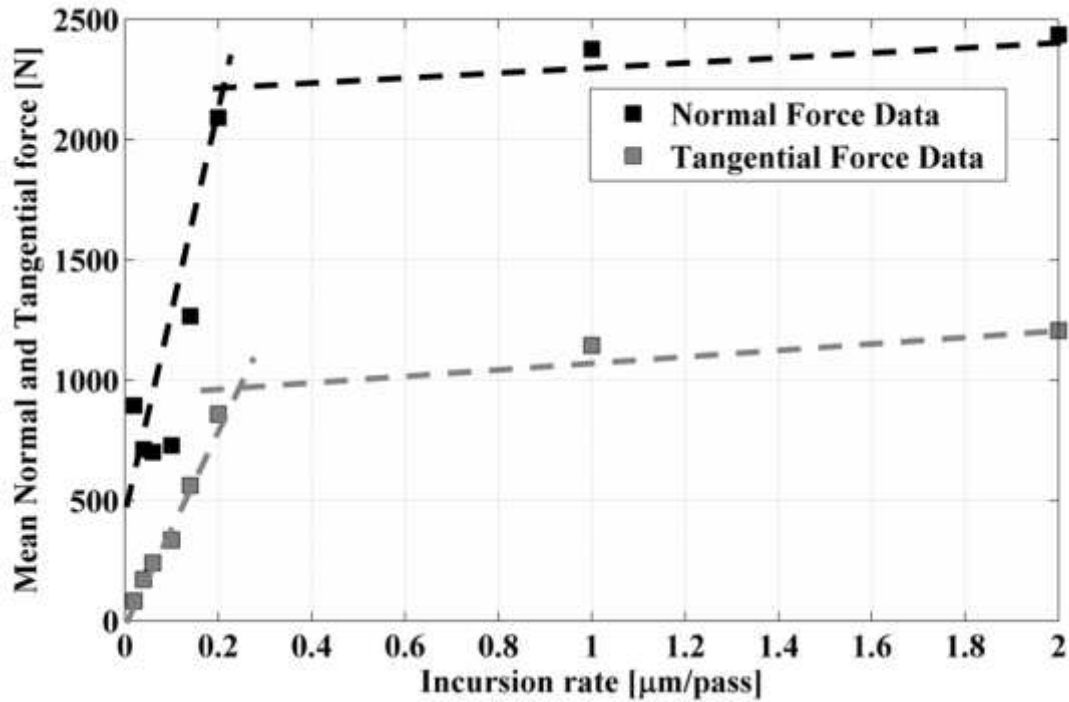


Figure 12. Average contact forces vs incursion rate.

Figure 12 shows the average normal and tangential forces as a function of incursion rate over the duration of a given test. Clearly due to the limitation of incursion depth, the overall rub length is different at each incursion condition. However, as demonstrated by Wang [9] in respect to a similar test platform, steady-state thermal conditions are quickly reached, and are done so within the range of rub lengths investigated in this study. Whilst significant variation in the two force components occurs during a test, both components show a similar average trend with respect to incursion rate. In both cases, force increases rapidly with incursion rate, before plateauing off and only showing a slow rate of increase at higher values of incursion rate. This result suggests that the material behaviour varies, and is different at high and low incursion rates. This point can be further explored by plotting the force ratio as a function of incursion rate (Figure 13). As shown in the figure, a transition point appears to occur in the force ratio at an incursion rate of 0.06 micrometers per pass. Indeed, the incursion rate is the same value at which the wear mechanism was observed to transition from adhesion to cutting, with Figure 13 appearing inverse in form when compared to the plot of adhesion rate as shown in Figure 9. At higher incursion rates, the measured force ratio is also similar to those found in orthogonal cutting of brittle materials [21, 22] and it is interesting to note that this corresponds to a well cut surface on the abradable material.

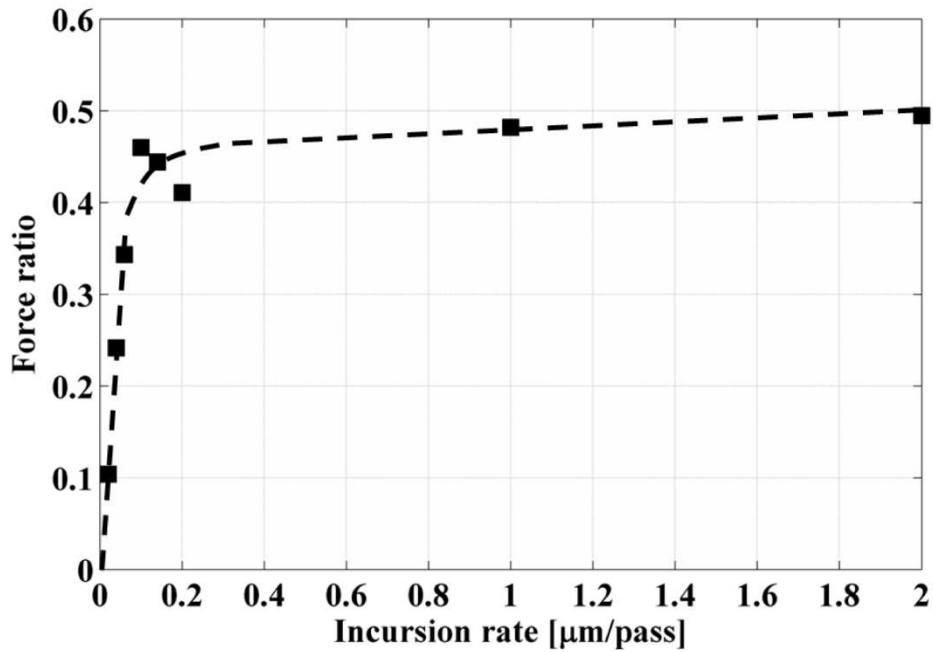


Figure 13. Force ratio vs incursion rate.

3.3 Post-Test Material Sections & Hardness Measurements

Whilst the primary focus of this investigation was the response of the abradable material, the hardness of the blade specimens post-test has been analysed using a Vickers micro-hardness tester (Mitutoyo, HM101 Series 810) with a load of 1 kg applied over a dwell time of 10 seconds. Tests were performed on longitudinally sectioned blade specimens, with measurements recorded at 0.5 mm intervals from the blade tip up to a maximum distance of 3 mm. Additionally a test was also performed on an un-used blade and a value of 370.70 ± 2.63 Hv recorded. In each case three repeat measurements were performed.

Incursion per pass [μm]	Average Hardness Post-Test [HV]
0.02	359.58 ± 6.51
0.06	354.03 ± 4.37
2	360.67 ± 5.64

Table 4. Hardness measure of the blades.

Average values of hardness for each blade are shown in Table 4. Values are reported in this way, as significant variation was not observed with respect to distance from the blade tip. As shown in the table, similar values were reported at all incursion rates, and whilst slightly

lower than the un-used value, would require further investigation to be deemed of significance.

In order to further investigate material behaviour, the abraded surface of the coating samples was sectioned. As discussed, this was performed in both the longitudinal and transverse direction with respect to the blade strike. Once prepared, the samples were inspected using an optical microscope. Figure 14a shows the microstructure of the coating; AlSi metal (white) and hexagonal boron nitride solid lubricant (dark grey) are visible, along with the porosity present in the coating (black). A further image at higher magnification is shown in Figure 14b, where the dark grey, lamellar, hexagonal boron nitride is clearly visible. The successful identification of the porosity in the coating also correlates well with that observed in previous studies [14], validating the sample preparation approach followed.

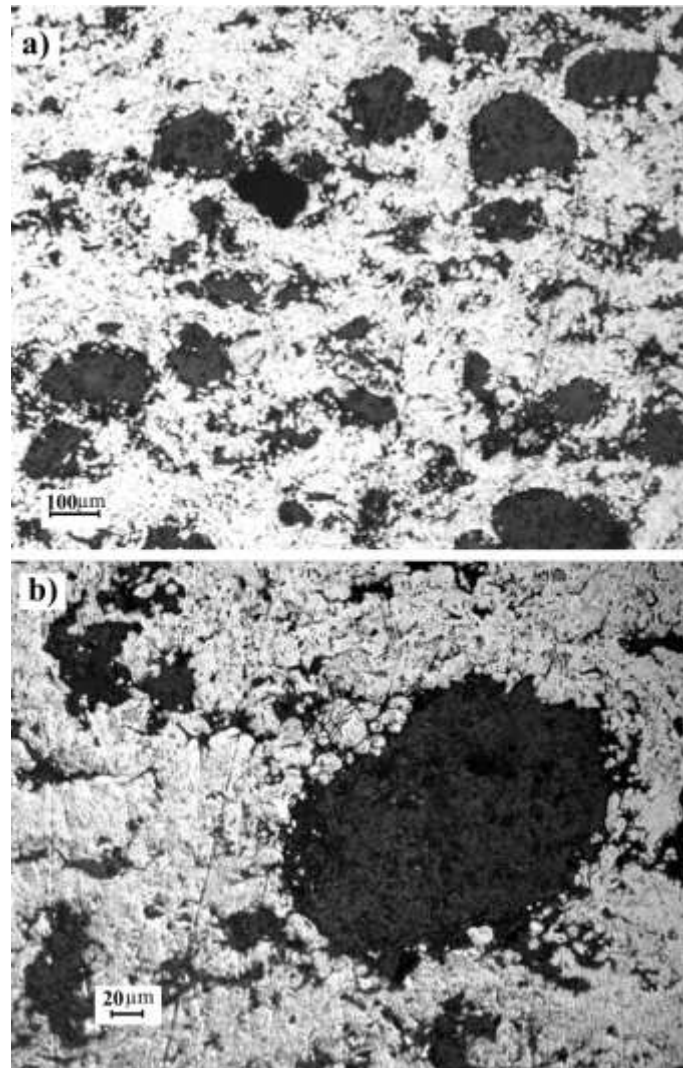


Figure 14. (a) microstructure of the AlSi-hBN (abradable material); (b) further magnification highlighting the presence of porosity (dark black) and lamellar hexagonal boron nitride.

Figure 15 shows longitudinal and transverse sections of the coating at an incursion rate of 0.02 micrometers per pass (Test 1). As shown by the longitudinal section in Figure 15a-b, significant compaction and solidification of the coating has occurred. This is shown by the distorted, fragmented hexagonal boron nitride phase in the near-surface, along with the more continuous AlSi phase at the surface itself. In particular, the solidified, continuous AlSi layer at the surface suggests melt wear of the coating, and represents a significant difference when compared to the as sprayed sample in Figure 16. It is also interesting to note that, as discussed, the highest temperatures were also recorded at this incursion rate (Table 1). The transverse section shown in Figure 15c has been taken at the location of the groove highlighted in Figure 7, which corresponded to thermal damage on the blade. As shown in the figure, compaction is significant, again evidenced by the nature of the boron nitride layer, with a large solidified layer also present. Conversely Figure 15d shows a transverse section taken from the trough of the groove as shown in the figure, compaction is similar to the peak of the groove, but solidification is reduced as evidenced by the increased hexagonal boron nitride phase in the near surface. On the corresponding point on the blade to the trough, no thermal damage was evident.

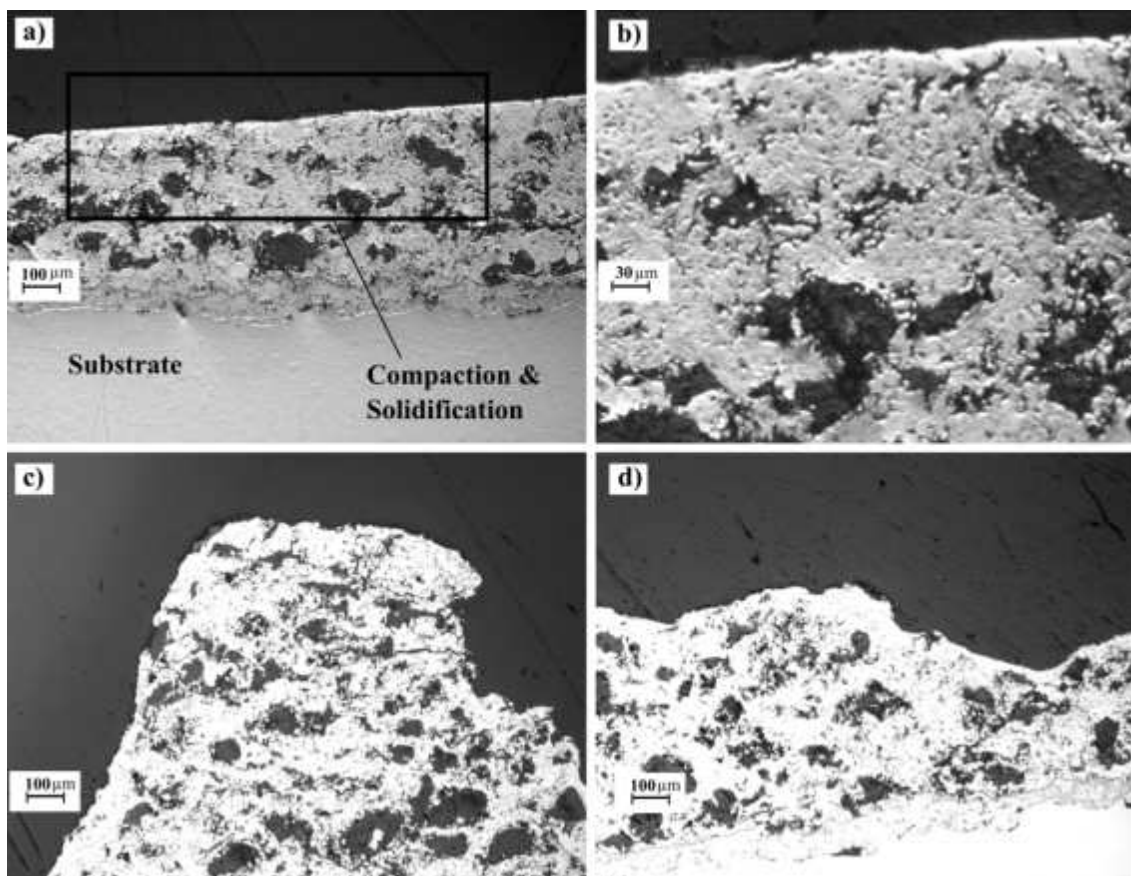


Figure 15. Section showing the microstructure of sub-surface at an incursion rate of $0.02 \mu\text{m}\cdot\text{pass}^{-1}$: a) longitudinal section; b) zoom of longitudinal section; c) transverse section corresponding to a groove peak; d) transverse section corresponding to a groove trough.

Figure 16 shows a high magnification image of the sectioned groove, along with the corresponding image of the coating surface. As shown in Figure 16a, material transfer appears to have occurred between the blade and the coating, with a corresponding dull area of transferred titanium present on the surface of the specimen (Figure 16b). This observation correlates well with the report of thermal damage at the corresponding point on the blade, and suggests that temperatures were locally hotter at this point on the coating when compared to other regions in the contact patch. Further, a crack is also evident on the coating, and is running perpendicular to the incursion and blade strike axes.

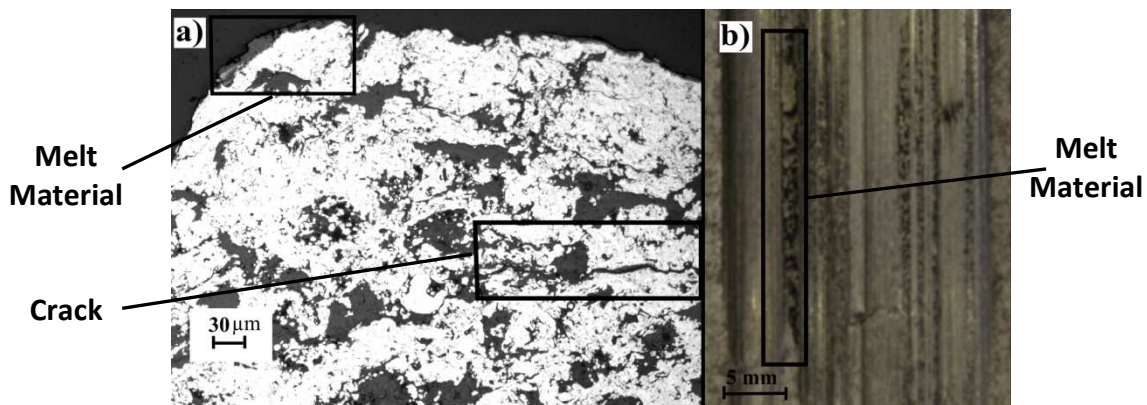


Figure 16. a) higher magnification image of groove region; b) coating after the test with melt material on the groove.

Figure 17, shows the microstructure of the coating at incursion rates of 0.2 and 2 micrometers per pass (Test 6 and 8 respectively). In these cases good cutting was observed for the abradable material, and is reflected in the microstructure. As shown in the figure, as the incursion rate is increased consolidation is minimal, with the intact hexagonal boron nitride phase remaining at the surface and little or no evidence of a solidified layer. This is particularly evident at the incursion rate of 2 micrometers per pass. In general, for both of these results the coating in the region close to the surface is smooth and well fractured, indicating an efficient cutting mechanism. However, the fact that minor consolidation is present at 0.2 micrometers per pass, does imply that an increase in cutting efficiency does occur with increasing incursion rate.

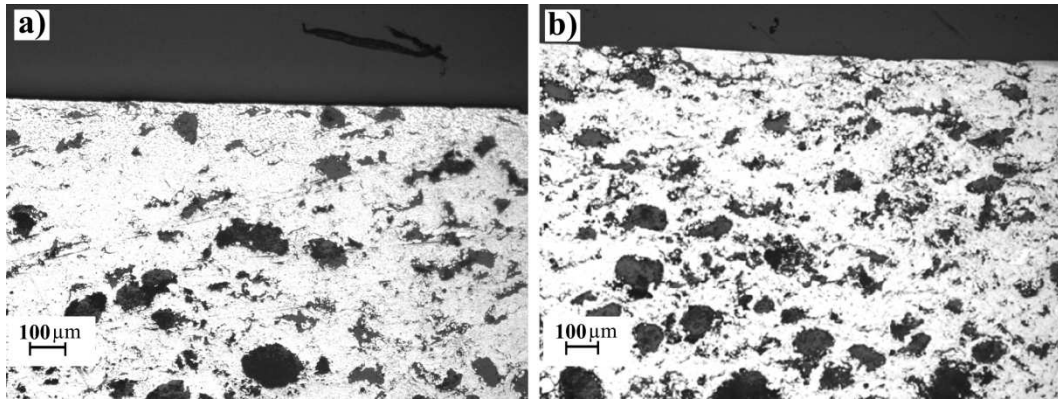


Figure 17. Section showing the microstructure on the longitudinal axis at an incursion rate: a) $0.2 \mu\text{m}\cdot\text{pass}^{-1}$; b) $2 \mu\text{m}\cdot\text{pass}^{-1}$.

Figure 18, shows the microstructure of the coating at an incursion rate of 0.06 micrometers per pass (Test 3). As shown in the figure, the coating is beginning to be well cut, with the solidified layer minimal, and the hexagonal boron nitride phase starting to occur intact at or close to the surface. This suggests that at or around this incursion rate, the material removal mechanism is transitioning, with a good cutting and dislocation of the abrasible material becoming dominant.

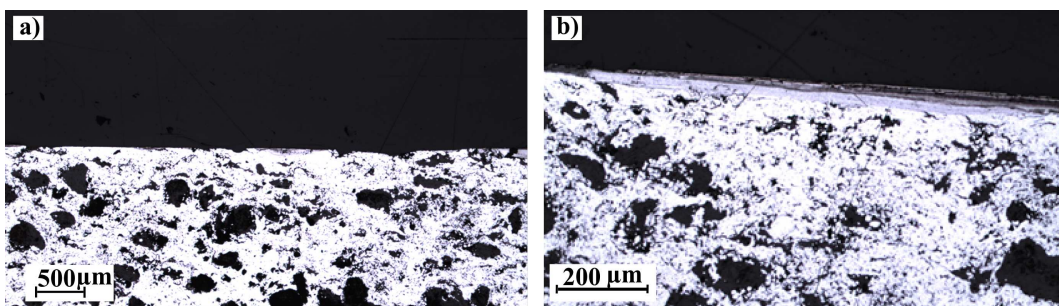


Figure 18. Section showing the microstructure on the longitudinal axis at an incursion rate $0.06 \mu\text{m}\cdot\text{pass}^{-1}$: a) low magnification, b) high magnification.

4. Discussion

The collective results for wear, cutting force and material structure post-incursion appear linked. In cases where adhesion has taken place, the extreme case being Test 1 performed at an incursion rate of 0.02 micrometers per pass, significant consolidation and solidification of the abrasible material has occurred. Previously, it has been suggested that at low incursion rates abrasible materials fail to dislocate effectively [2], and that appears to be the case here. The presence of solidification implies high surface temperatures, and the presence of a melt layer between the blade and abrasible material. Whilst flash temperatures in the contact were not measured, the highest average surface temperature was measured for the lowest incursion

rate. It is also interesting to note that when investigating an area corresponding to thermal damage on the blade, significant solidification was present and blade material has been transferred to the coating. At these conditions the ratio of tangential to normal force is also low, implying a low resistance to tangential motion. This result is in keeping with consolidation as opposed to cutting of the abradable material, along with a low friction melt layer at the surface. The fact adhesion has taken place, and in the case of this test that the blade length change and force curves are similar in form (Figure 8a, 10a, and 11a respectively), supports this view.

Conversely, at high incursion rate, the material is observed to dislocate and cut well. At an incursion condition of 2 micrometers per pass (Test 8), the microstructure shows little sign of consolidation or solidification, with no thermal damage present on the blade. Similarly, results for blade length change show negligible adhesion with slight blade wear present, with the force ratio also higher. The force ratio recorded suggests a cutting mechanism, where the blade encounters significant tangential resistance as it fractures the material. The efficiency of this mechanism is further reinforced by the fact that whilst overall forces are higher than at low incursion rate, average temperatures were lower, and thermal damage to the blade or abradable is not present.

The close relationship between material behaviour, wear and cutting force is again highlighted by Figures 9 and 13, which show the adhesion rate and force ratio respectively as a function of incursion rate. These results indicate a sliding scale, whereas incursion rate increases, the material cuts more efficiently, resulting in reducing adhesion and an increasing force ratio. This result is highlighted by the microstructures shown in Figures 15 and 17, where a transition in material behaviour is observed with incursion rate. The results from this study also show that at an incursion rate of 0.06 micrometers per pass, cutting begins to dominate for this coating. The force ratio defined is an indication of the mechanical behaviour of the blade / abradable system, and ultimately how the abradable dislocates, and has the potential to be used in the modelling of this system, in much the same way as cutting force ratios are used for turning, milling, and grinding.

5. Conclusion

A series of tests have been performed over a range of incursion rates, and the wear behaviour, contact forces and material behaviour have been investigated. The study shows that material behaviour is strongly dependent on the incursion rate, with low incursion rates resulting in low tangential forces and adhesion, and high incursion rates resulting in higher forces and good cutting. A transition was observed to occur between these two mechanisms as incursion rate was increased, with an incursion per pass of 0.06 micrometers identified as a threshold below which adhesive behaviour was observed.

References

- [1] Stringer J., Marshall M.B. High speed wear testing of an abradable coating. *Wear* 2012; 294-295: 257-263.
- [2] Fois N., Stringer J., Marshall M.B., Adhesive transfer in aero-engine abradable linings contact. *Wear* 2013; 304: 202-210.
- [3] Austin Spang III H., Brown Harold. Control of jet engines. *Pergamon Control Engineering Practice* 1999; 1043-1059.
- [4] Sporer D., Wilson S., Giovanetti I., Refke A., Giannozzi M. On the potential of metal and ceramic based abradables in turbine seal application. *Proceedings of the Thirty-Sixth Turbomachinery Symposium* 2007, Texas A&M University, pp. 79-86.
- [5] Faraoun H.I., Grosdidier T., Seichepine J.L., Goran D., Aourag H., Coddet C., Zwick J., Hopkins N. Improvement of thermally sprayed abradable coating by microstructure control. *Surface and Coating Technology* 2006; 201: 2303-2312.
- [6] Johnston R.E. Mechanical characterisation of AlSi-hBN, NiCrAl-Bentonite, and NiCrAl-Bentonite-hBN freestanding abradable coatings. *Surface and Coatings Technology* 2011; 205: 3268-3273.
- [7] Bounazef M., Guessasma S., Ait Saadi B. The wear, deterioration and transformation phenomena of abradable coating BN-SiAl-bonding organic element, caused by the friction between the blades and the turbine casing. *Materials Letters* 2004; 58: 3375-3380.
- [8] Wang H. Criteria for analysis of abradable coatings. *Surface and Coatings Technology* 1996; 79: 71-75.

- [9] Wang H. An Analysis of Turbine Blade/Abradable Seal Rubbing, in H. Henein and T. Oki (eds), *Proc. 1st Int. Conf. on Processing Materials for Properties, Honolulu, HI*, 1993, Minerals, Metals and Materials Society, pp. 1085-1088.
- [10] Yi M., He J., Huang B., Zhou H. Friction and wear behaviour and abradability of abradable seal coating. *Wear* 1999; 231: 47-53.
- [11] Padova C., Barton J., Dunn M. G., Manwaring S., Young G, Adams M. L. and Adams M., Development of an Experimental Capability to Produce Controlled Blade Tip/Shroud Rubs at Engine Speed. *Journal of Turbomachinery*, 2005, 127, 726-735.
- [12] Padova C., Dunn M. G., Barton J. Casing treatment and blade tip configuration effects on controlled gas turbine blade tip/shroud rubs at engine conditions. *Proceedings of ASME Turbo Expo 2008: Power for Land, Sea and Air, GT2008*, June 9-13, 2008, Berlin, Germany.
- [13] Baiz S., Fabis J., Boidin X., Desplanques Y. Experimental investigation of the blade/seal interaction, *Proc IMechE Part J: J. Engineering Tribology* 2013; 227: 980-995.
- [14] Matejicek J., Kolman B., Dubsky J., Neufuss K., Hopkins N., Zwick J. Alternative methods for determination of composition and porosity in abradable materials. *Materials Characterization* 2006; 57: 17-29.
- [15] Glancy S.D. Universal Metallographic Procedure for Thermal Spray Coatings. *Structure. Struers Journal of Materialography* 1996, 29:12-16.
- [16] Blann G. A. Metallographic specimen preparation of thermally sprayed coating for microstructural analysis. *Microstructural Science, IMS and ASM International, Metals Park, OH*, 1989; 17: 139-151.
- [17] Vander Voort G. F. Metallography Principles and Practice, *McGraw-Hill*, 1984, pp. 267-318.
- [18] Ahrens J, Ulbrich H, Ahaus G. Measurement of contact forces during blade rubbing. *Vibration in Rotating Machinery, 7th International Conference*, Nottingham, September 12-14 2000, ImechE, London, pp. 259-263.
- [19] Ricardo Castro L., Vieville P., Lipinski P., Correction of dynamic effects on the force measurements made with piezoelectric dynamometers. *International Journal of Machine Tools & Manufacture*, 2006; 46: 1707-1715.

[20] Tounsi, N., Otho, A. Dynamic cutting force measuring. *International Journal of Machine Tools & Manufacture*, 2000; 40; 1157-1170.

[21] San-Juan M., Martin O., Santos F. Experimental study of friction from cutting forces in orthogonal milling. *International Journal of Machine Tools & Manufacture* 2010; 50: 591-600.

[22] Grzesik W. *Advanced Machining Processes of Metallic Materials, Theory, Modelling and Applications*. Elsevier, 2008, pp. 149-160.